

# Structural analyses of RuO<sub>2</sub>–TiO<sub>2</sub>/Ti and IrO<sub>2</sub>–RuO<sub>2</sub>–TiO<sub>2</sub>/Ti anodes used in industrial chlor-alkali membrane processes

Yoshio Takasu · Wataru Sugimoto ·

Yoshinori Nishiki · Shuji Nakamatsu

Received: 29 January 2010 / Accepted: 13 April 2010 / Published online: 29 April 2010  
© Springer Science+Business Media B.V. 2010

**Abstract** The morphology and composition of RuO<sub>2</sub>–TiO<sub>2</sub>/Ti and IrO<sub>2</sub>–RuO<sub>2</sub>–TiO<sub>2</sub>/Ti anodes, which have been used for the production of chlorine for more than 10 years, were analyzed by various methods; such as high-resolution scanning electron microscopy, high-resolution Auger electron spectroscopy, electron probe X-ray emission micro-analysis and X-ray diffraction analysis. Drastic changes in the surface morphology, including partial exfoliation of a small amount of the oxide layer and a reduction in the content of ruthenium species through dissolution, were observed for the RuO<sub>2</sub>–TiO<sub>2</sub>/Ti anode. For the IrO<sub>2</sub>–RuO<sub>2</sub>–TiO<sub>2</sub>/Ti anode, on the other hand, there were moderate changes in the surface morphology and moderate dissolution of iridium and ruthenium species.

**Keywords** Iridium oxide · Ruthenium oxide · Titanium oxide · Anode · Chlorine evolution

## 1 Introduction

The electrolysis of brine, a concentrated aqueous solution of sodium chloride, used for the production of chlorine, sodium hydroxide and hydrogen, is an important industrial electrochemical process. Since the anode of the electrolysis process is exposed to a highly oxidative environment in a weak acid solution during the electrolysis, anti-corrosive

oxide-coated dimensionally stable anodes, called DSA® or DSE®, have usually been used worldwide. After the development of the DSA® [1], both fundamental and applied researches have been carried out as reviewed by Trasatti [2–4]. For instance, industrial applications for chlor-alkali processes [5–11]; the form of Ti substrates (e.g. nets, meshes, expanded metals) of the DSA®'s used in industry [8–11]; the optimum chemical composition such as RuO<sub>2</sub>–TiO<sub>2</sub>/Ti (30–70%) [12–14]; recommended preparation temperature (e.g. 400–500 °C for RuO<sub>2</sub>–TiO<sub>2</sub>/Ti) [13, 15]; surface area (roughness factor) of oxide electrodes such as IrO<sub>2</sub>–RuO<sub>2</sub>/Ti electrodes [16–18]; observation of the mud-cracks by scanning electron microscopy (SEM) [19, 20]; effect of the preparation conditions on the formation of solid–solution (e.g. RuO<sub>2</sub>–TiO<sub>2</sub>/Ti) [21, 22]; observation of the enrichment of the surface with particular species such as TiO<sub>2</sub> or IrO<sub>2</sub> by electron spectroscopy [23–27]; effect of IrO<sub>2</sub>–RuO<sub>2</sub> or RuO<sub>2</sub>–TiO<sub>2</sub> on the durability of the DSA®'s [16–18, 27–31]; preparation of oxide powders such as RuO<sub>2</sub>–TiO<sub>2</sub>, IrO<sub>2</sub>–RuO<sub>2</sub>–TiO<sub>2</sub> and IrO<sub>2</sub>–RuO<sub>2</sub> to clarify the stable crystal structure of the binary and ternary oxides [32–34]; single-crystal oxide electrodes, RuO<sub>2</sub> for example, to investigate the real catalytic property of oxide electrodes [35]; oxygen evolution activity of IrO<sub>2</sub> for the electro-plating [3, 36–41]. The morphology, crystal structure, and composition of DSA®-type electrodes have been characterized by many research scientists; however, the precise durability of the anodes used in industry has not yet been determined. Typical DSA®'s used in chlor-alkali processes are RuO<sub>2</sub>–TiO<sub>2</sub>/Ti and IrO<sub>2</sub>–RuO<sub>2</sub>–TiO<sub>2</sub>/Ti, in which both ruthenium and iridium species act as catalysts for the chlorine evolution and iridium enhances the durability of the RuO<sub>2</sub>–TiO<sub>2</sub> oxide layer.

In the present investigation, the oxide layers of RuO<sub>2</sub>–TiO<sub>2</sub>/Ti and IrO<sub>2</sub>–RuO<sub>2</sub>–TiO<sub>2</sub>/Ti anodes, which were

Y. Takasu (✉) · W. Sugimoto  
Department of Materials and Chemical Engineering, Shinshu University, 3-15-1 Tokida, Ueda, Nagano 386-8567, Japan  
e-mail: ytakasu@shinshu-u.ac.jp

Y. Nishiki · S. Nakamatsu  
Permelec Electrode Ltd, 2023-15 Endo, Fujisawa, Kanagawa 252-0816, Japan

applied in two different electrolytic cells, were characterized and compared with those of pristine specimens. The information on these typical DSA®'s must contribute to not only the improvement of DSA®'s but also to the design of new oxide-coated electrocatalysts.

## 2 Experimental

### 2.1 Test electrodes

Optical micrographs of the RuO<sub>2</sub>–TiO<sub>2</sub>/Ti and the IrO<sub>2</sub>–RuO<sub>2</sub>–TiO<sub>2</sub>/Ti anodes analyzed in this investigation are shown in Fig. 1. Both electrodes have a characteristic low overpotential for chlorine evolution in chlor-alkali membrane cells. The RuO<sub>2</sub>–TiO<sub>2</sub>/Ti electrode has been used for 12 years at average current density of 4 kA m<sup>-2</sup>. The IrO<sub>2</sub>–RuO<sub>2</sub>–TiO<sub>2</sub>/Ti electrode with an initial molar ratio of Ir:Ru = 1:1 has been used for 15 years of the chlorine evolution in industry at average current density of 3 kA m<sup>-2</sup>. For both electrodes, the parts that were not exposed to the electrolyte were regarded as pristine specimens in this study. In this investigation, the surface of the anodes facing the membrane during the electrolysis was analyzed.

### 2.2 Characterization methods of the electrodes

The morphology and the composition of the electrode specimens were analyzed by high-resolution scanning electron microscopy (HR-SEM; Hitachi S-5000), high-resolution Auger electron spectroscopy (HR-AES; Physical Electronics Inc, Model 680). The diameter of the incident electron beam was 35 nm. Evaluation of the elements, Ti-LMM Auger peaks, Ir-MNN Auger peaks, Ru-MNN, LMM Auger peaks), and electron probe X-ray emission microanalysis (EPMA, JEOL, JXA-8600MX). The crystal structure of the oxide layer of the electrodes was

characterized by X-ray diffraction analysis (XRD, Rigaku RINT-2550, CuK<sub>α</sub>).

## 3 Results and discussion

### 3.1 The RuO<sub>2</sub>–TiO<sub>2</sub>/Ti electrode

#### 3.1.1 Morphology of the oxide layer

Figure 2 shows HR-SEM images at various magnifications of the surface of the pristine RuO<sub>2</sub>–TiO<sub>2</sub>/Ti electrode. The following morphological characteristics were observed, (1) an apparently flat part, (2) crystallites with 50 nm–2 μm in diameter scattered on the flat part, and (3) mud-cracks. Even the apparently flat surface observed at lower magnifications was composed of small connected particles that formed narrow apertures (Fig. 2d).

After used for 12 years, the anode showed drastic changes in the surface morphology (Fig. 3): partial exfoliation of the surface layer occurred at various places, crystallites with 50 nm–2 μm in diameter on the flat part disappeared, and small crystallites with 20–60 nm in diameter were exposed on the exfoliated part. Figure 4 is cross-sectional SEM images of the pristine and the used anodes. A stacked oxide with 20 layers was clearly observed on both SEM images. The number of the stacked layers corresponds to the coating times. Thus, the layered oxide structure of these anodes was almost maintained even after the 12 year anodic polarization. The black part “G” shown in Fig. 4a is a gap formed, as a result of the cross-sectional cutting, between the oxide layer and the Cu layer which was plated onto the RuO<sub>2</sub>–TiO<sub>2</sub>/Ti electrode to stabilize the oxide layer towards the cross-sectional cutting.

In the case of the used anode, a few voids smaller than 1 μm in diameter are observed (Fig. 4). Although the smaller voids were also observed in the oxide layer of the

**Fig. 1** The RuO<sub>2</sub>–TiO<sub>2</sub>/Ti and IrO<sub>2</sub>–RuO<sub>2</sub>–TiO<sub>2</sub>/Ti anodes.

**a** RuO<sub>2</sub>–TiO<sub>2</sub>/Ti; expanded Ti mesh. **b** IrO<sub>2</sub>–RuO<sub>2</sub>–TiO<sub>2</sub>/Ti; circularly perforated Ti plate

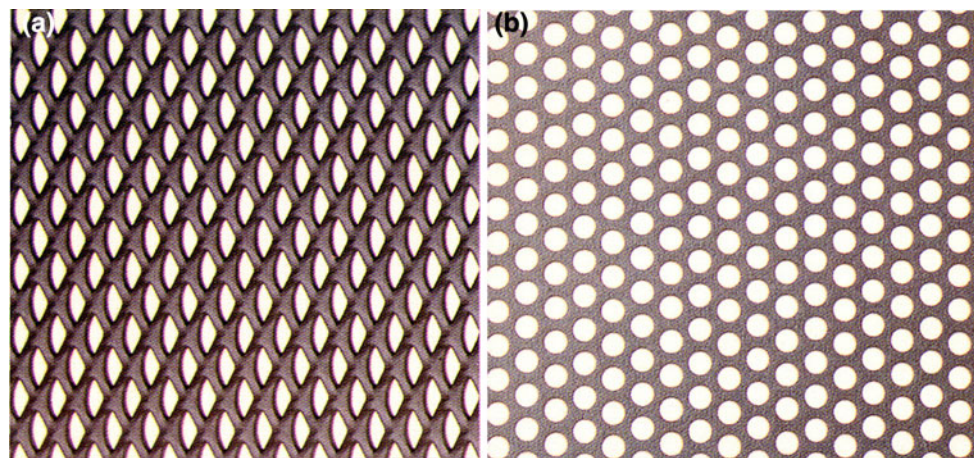


**Fig. 2** HR-SEM images at various magnifications of the pristine RuO<sub>2</sub>–TiO<sub>2</sub>/Ti anode

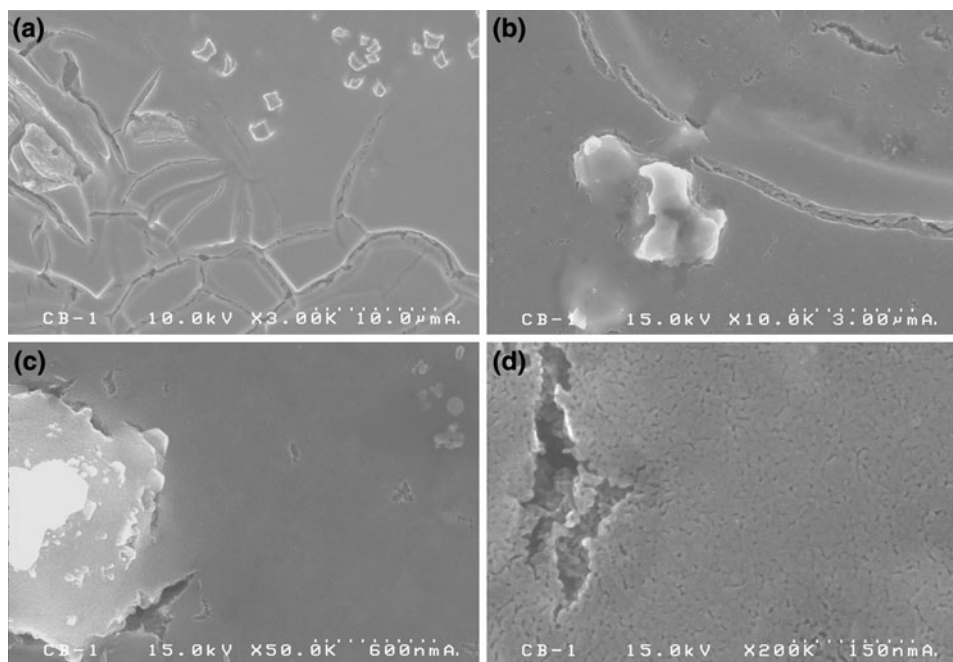
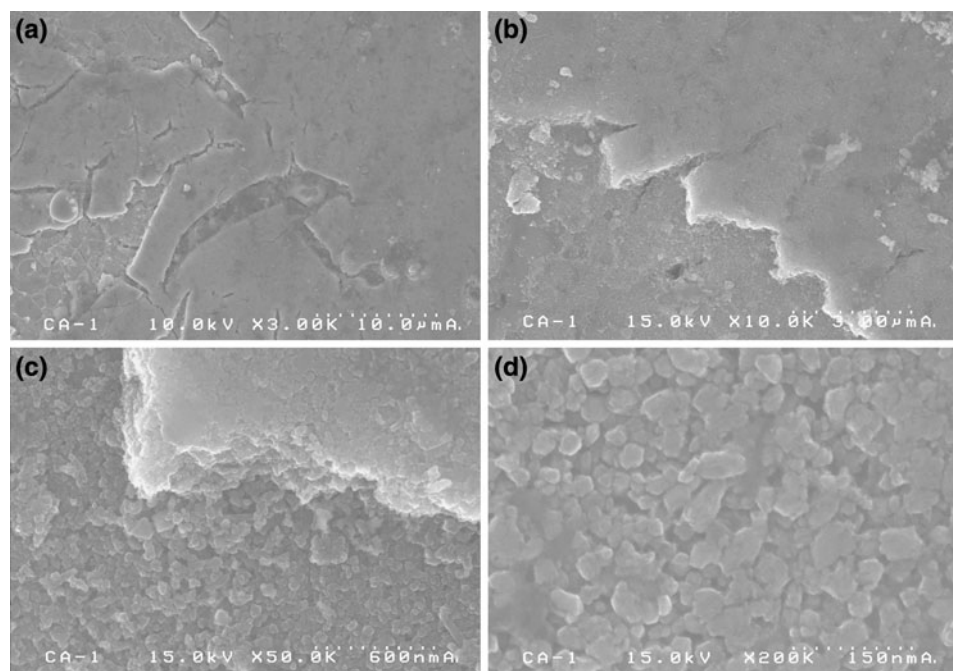


**Fig. 3** HR-SEM images at various magnifications of the RuO<sub>2</sub>–TiO<sub>2</sub>/Ti anode used for 12 years



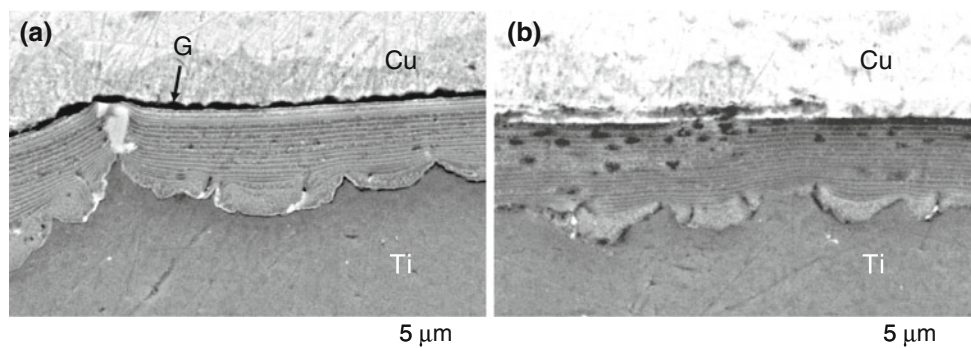
pristine electrode, the voids observed in the used anode must have been formed through the dissolution of oxide species during electrolysis. Thus, the dissolution of the oxide species must have occurred not only from the surface but also from inner part of the oxide layer.

### 3.1.2 Composition and structure of the oxide layer

Figure 5 shows the SEM images with the point analysis data determined by the HR-AES for the pristine and the

used anodes. The quantitative analysis of the content of ruthenium, titanium and oxygen is difficult due to the heterogeneity in the composition. The elements detected by the spot analysis are presented only for the characteristic parts. In every crystallite on the pristine electrode, Ru, Ti and O were detected, while no appreciable amount of Ru was detected on the flat part. The enrichment of the titanium oxide on the surface of the flat part must be caused, at least partially, not only by the higher reactivity of titanium precursor than that of ruthenium precursor but also by the

**Fig. 4** Cross-sectional SEM images of the pristine and used RuO<sub>2</sub>–TiO<sub>2</sub>/Ti anodes. **a** Pristine. **b** Used for 12 years. The RuO<sub>2</sub>–TiO<sub>2</sub>/Ti anodes were coated with copper to stabilize the oxide layer towards the cross-sectional cutting. The mark “G” in the left SEM image indicates the gap between the oxide layer and the Cu layer formed by the cross-sectional cutting process



diffusion of titanium ions from the titanium substrate. On the other hand, Ru was not detected anywhere on the used electrode by the HR-AES. Even though no Ru species existed in the surface layers, the electrode is still active for the chlorine evolution. This suggests that the electrolyte reaches the Ru sites in the inner layer of the porous anode where the electrolysis proceeds. The EPMA analysis of the oxide layer before and after the polarization showed that the 12 year anodic polarization resulted in considerable loss of ruthenium of up to 43% from the RuO<sub>2</sub>–TiO<sub>2</sub> layer.

The XRD patterns of the electrode before and after the polarization are shown in Fig. 6. No evident decrease in the intensity of the diffraction peaks from the oxide by the polarization was observed. No shift of the diffraction peaks was observed even after the 12 years polarization.

### 3.2 The IrO<sub>2</sub>–RuO<sub>2</sub>–TiO<sub>2</sub>/Ti electrodes

#### 3.2.1 Morphology of the oxide layer

Figure 7 shows HR-SEM images of the surface of the pristine IrO<sub>2</sub>–RuO<sub>2</sub>–TiO<sub>2</sub>/Ti electrode at various magnifications. The surface was heterogeneous in morphology and composed of granules with a few micrometers in diameter and needle-like crystallites grown both on the granules and from the aperture

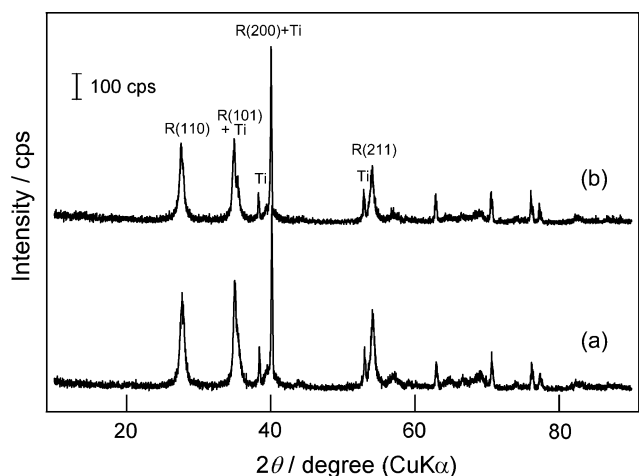


**Fig. 6** X-ray diffraction patterns of the pristine and the used RuO<sub>2</sub>–TiO<sub>2</sub>/Ti anodes. **a** Pristine. **b** Used for 12 years

of each granule. Even apparently flat granules at lower magnifications were composed of small connected particles, ca. 10–20 nm in diameter, which formed narrow apertures and cracks. The needle-like crystallites, clarified at the higher magnification, were square columnar crystallites (Fig. 7c). The HR-SEM images of the anode used for 15 years showed that a drastic change in the surface morphology occurred as a

**Fig. 5** SEM images with the point analysis data determined by the HR-AES for the pristine and the used RuO<sub>2</sub>–TiO<sub>2</sub>/Ti anodes. **a** Pristine. **b** Used for 12 years. Analyzed part by the HR-AES: **a** 1, 3; crystallites, 4, 2; flat part, **b** 1, 2; hollow part, 3, 4; flat part

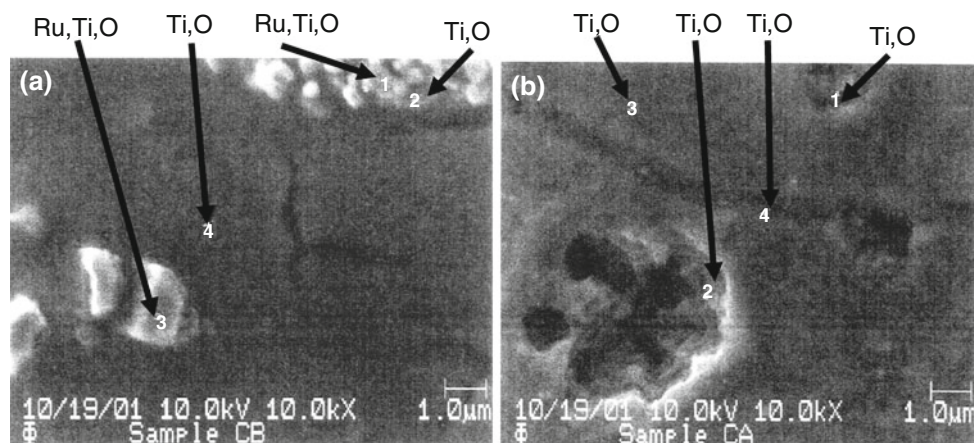


**Fig. 7** HR-SEM images at various magnifications of the pristine  $\text{IrO}_2\text{-RuO}_2\text{-TiO}_2/\text{Ti}$  anode

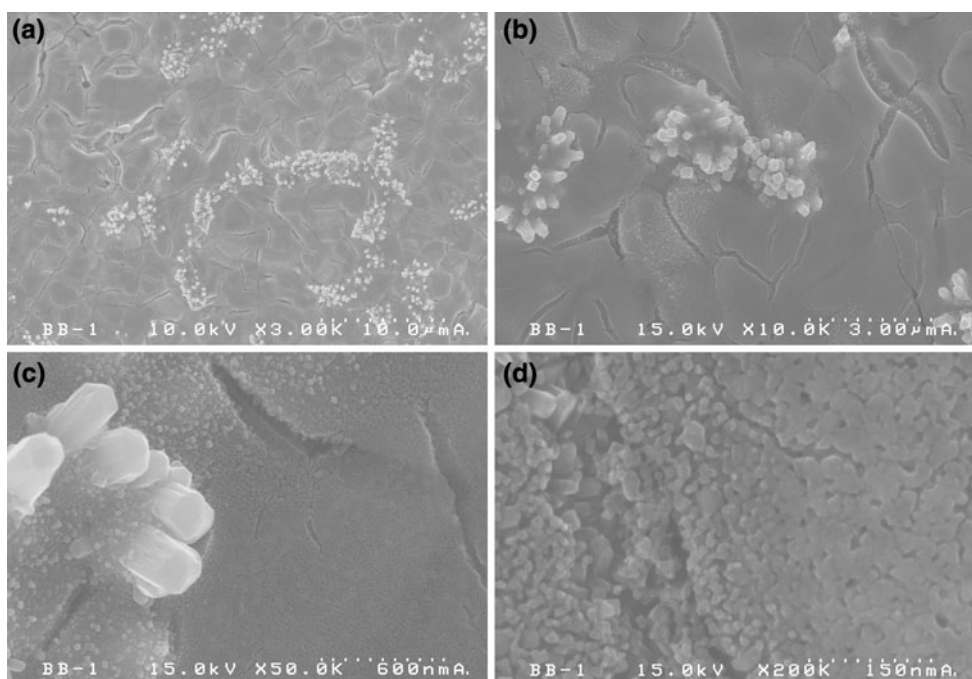
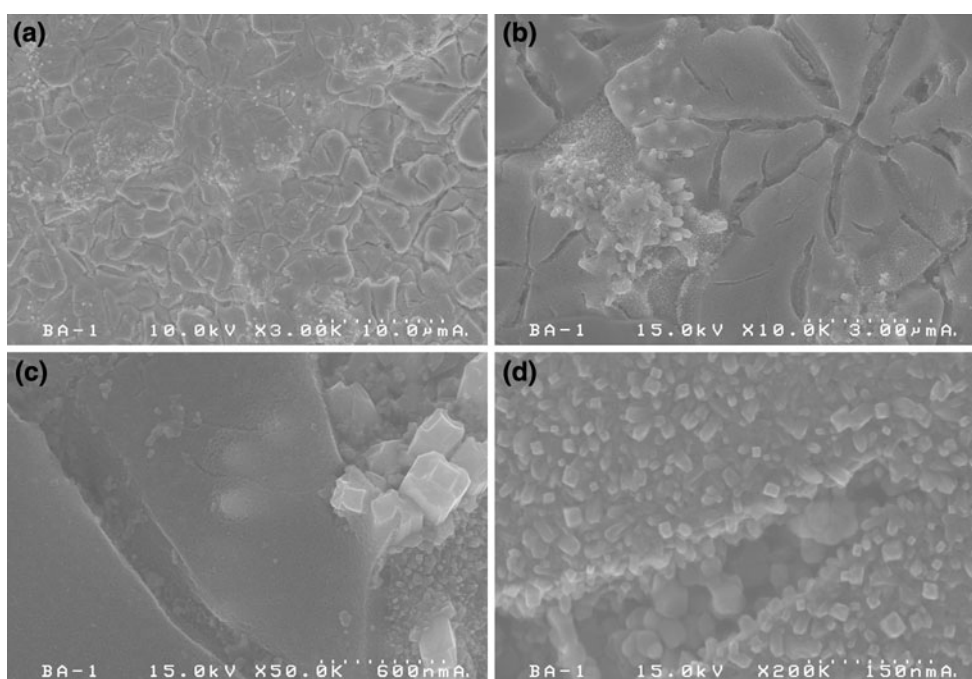


**Fig. 8** HR-SEM images at various magnifications of the  $\text{IrO}_2\text{-RuO}_2\text{-TiO}_2/\text{Ti}$  anode used for 15 years



result of polarization (Fig. 8). In other words, the granules and square columnar crystallites with 10–30 nm in diameter became evident, so did the corrosion of the edges of the square columnar crystallites.

In Fig. 9, a cross-sectional SEM image of the pristine anode is compared with the polarized one. Unlike the case of the  $\text{RuO}_2\text{-TiO}_2/\text{Ti}$  electrode, the layered oxide structure was unclear except for that near the surface of the pristine electrode. Although a few layers near the surface of the

pristine electrode were dark-gray, the dark-gray layer increased to about one-third of the width of the oxide-coating in the polarized one. Thus, the selective dissolution of the conductive component of the oxide-coating proceeded by the 15 years polarization must be responsible for the increase in the width of the dark-gray layer, while the difference in the composition for the two layers, shown as white and dark-gray layers in the SEM image, has not been characterized.

**Fig. 9** Cross-section SEM images of the pristine and used  $\text{IrO}_2\text{-RuO}_2\text{-TiO}_2/\text{Ti}$  anodes. **a** Pristine. **b** Used for 15 years. The  $\text{IrO}_2\text{-RuO}_2\text{-TiO}_2/\text{Ti}$  anodes were coated with copper to stabilize the oxide layer towards the cross-sectional cutting

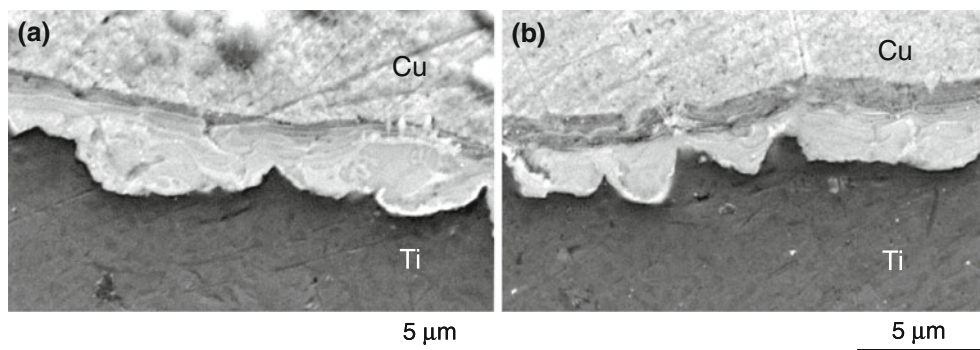


**Fig. 10** SEM images with the point analysis data determined by the HR-AES for the pristine and the used  $\text{IrO}_2\text{-RuO}_2\text{-TiO}_2/\text{Ti}$  anodes. **a** Pristine. **b** Used for 15 years. Analyzed part by the HR-AES: **a** 1, 3; crystallites, 2; flat part, 4; crystallites in a crack, **b** 1, 3; crystallites, 2, 4; flat part

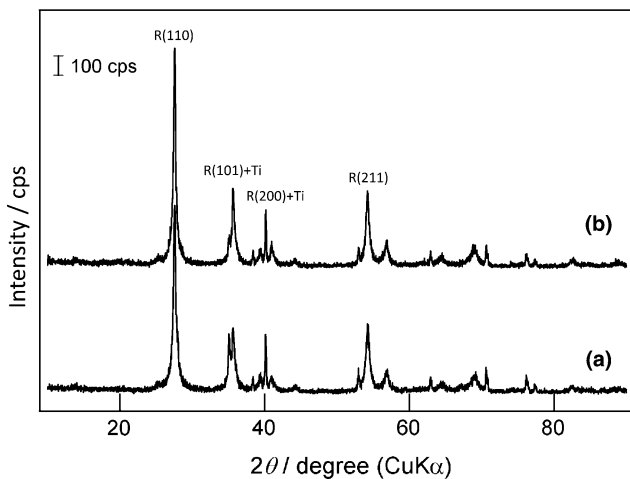
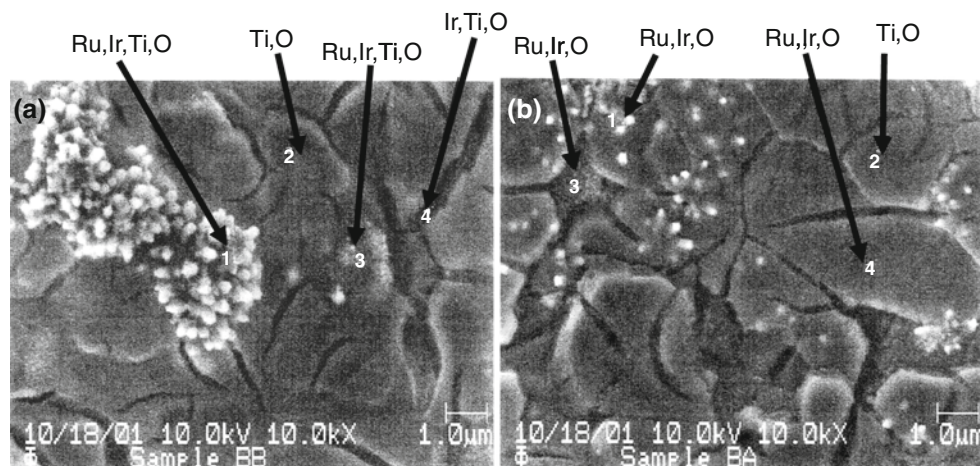


**Fig. 11** X-ray diffraction patterns of for the pristine and the used  $\text{IrO}_2\text{-RuO}_2\text{-TiO}_2/\text{Ti}$  anodes

### 3.2.2 Composition and structure of the oxide layer

Figure 10 shows SEM images with the point analysis data determined by the HR-AES for the pristine and the used  $\text{IrO}_2\text{-RuO}_2\text{-TiO}_2/\text{Ti}$  anode. In every crystallite on the pristine electrode, Ir, Ru, Ti and O were detected, while no appreciable amounts of Ir and Ru were detected on the flat

part. The enrichment of the titanium oxide on the flat part must be caused, at least partially, not only by the higher reactivity of titanium precursor than those of the other metal precursors but also by the diffusion of titanium ions from the titanium substrate. Differently from the case of the  $\text{RuO}_2\text{-TiO}_2/\text{Ti}$  anode, precious elements could be detected anywhere after the polarization on the used electrode, with the exception of some parts analyzed by the HR-AES. The EPMA analysis of the oxide layer before and after polarization showed that the 15 years anodic polarization caused slight losses of iridium (15%) and ruthenium (14%) from the  $\text{IrO}_2\text{-RuO}_2\text{-TiO}_2$  layer.

The XRD patterns of the electrode before and after the polarization are shown in Fig. 11. No evident decrease in the intensity of the diffraction peaks from the oxide was observed. No evident shift of the diffraction peaks was observed even after the 15 years polarization.

## 4 Summary

The surface morphology, cross-section profile, and composition of the oxide layer of  $\text{RuO}_2\text{-TiO}_2/\text{Ti}$  and those of  $\text{IrO}_2\text{-RuO}_2\text{-TiO}_2/\text{Ti}$  anodes, which have been used for the industrial production of chlorine for 12 and 15 years,

respectively, were characterized by various methods. For the RuO<sub>2</sub>–TiO<sub>2</sub>/Ti anode, considerable dissolution of ruthenium species (43%) and partial exfoliation of the oxide layers were observed. Although the layered oxide structure of the anode was almost maintained, some amount of dissolution of the oxide species from the inner layer was observed, forming voids with smaller than 1 μm in diameter. For the IrO<sub>2</sub>–RuO<sub>2</sub>–TiO<sub>2</sub>/Ti anode, a slight loss of the content of iridium (15%) and ruthenium (14%) was observed. The square columnar crystallites on the surface were also somewhat etched by the lengthy anodic polarization. The cross-sectional SEM image of the anode polarized for 15 years suggested the altered region by the selective dissolution of the conductive component of the oxide-coating. The information on the structural analyses for these typical DSA®'s used for more than 10 years in industries must contribute to not only the improvement of DSA®'s but also to the design of new oxide-coated electrocatalysts.

**Acknowledgments** The authors are grateful to Shinko Electronic Industrial Co Ltd for obtaining the HR-AES spectra.

## References

1. Beer HB (1965) British Patent 1,147,442
2. Trasatti S (2000) *Electrochim Acta* 45:2337
3. Trasatti S (2000) *Electrochim Acta* 36:225
4. Trasatti S (1999) In: Wiekowski A (ed) *Interfacial electrochemistry: theory, practice, applications*. Marcel Dekker, New York
5. De Nora O (1970) *Chem Ing Tech* 42:222
6. Beer HB (1980) *J Electrochem Soc* 127:301C
7. Nishiki Y, Nakamatsu S, Aoki K, Tokuda K (1989) *J Appl Electrochem* 19:90
8. Horacek J, Puschver S (1971) *Chem Eng Prog* 67:71
9. De Nora O (1971) *Chem Ing Tech* 43:182
10. Nidola A (1981) In: Trasatti S, Lodi G (eds) *Electrodes of conductive metallic oxides, part B*. Elsevier, Amsterdam, p 627
11. Koziol KR, Sieberer KH, Rathjen HC, Zenk JB, Wenk EF (1977) *Chem Ing Tech* 49:288
12. Cominellis Ch, Vercesi GP (1991) *J Appl Electrochem* 21:136
13. Hine F, Yasuda M, Yoshida T (1977) *J Electrochem Soc* 124:500
14. Veselovskaya IE, Spasskay EK, Sokolov VA, Tkachenko VI, Yakimenko LM (1974) *Sov Electrochim* 10:62
15. Burke LD, Murphy OJ (1979) *J Electroanal Chem Interfacial Electrochem* 96:19
16. Yeo RS, Orehotsky J, Visscher W, Srinivasan S (1981) *J Electrochem Soc* 128:1900
17. Roginskaya YE, Varlamova TV, Goldstein MD, Belova ID, Galyamov BS, Shifrina RR, Shepelin VA, Fateev VN (1991) *Mater Chem Phys* 30:101
18. Savinell RF, Zeller RL III, Adams JA (1990) *J Electrochem Soc* 137:489
19. Pizzini S, Buzzanca G, Mari C, Rossi L, Torchio S (1972) *Mater Res Bull* 7:449
20. Barral G, Guitton J, Montella C, Vergara F (1977) *Surf Technol* 6:39
21. Angelinetta C, Trasatti S, Atanasoska LD, Minevski ZS, Atanasoski RT (1989) *Mater Chem Phys* 22:231
22. Gerrard WA, Steele BCH (1978) *J Appl Electrochem* 8:417
23. Atanasoska Lj, Atanasoski RT, Trasatti S (1990) *Vacuum* 40:91
24. Kondintsev IM, Trasatti S, Rubel M, Wieckowski A, Kaufher N (1992) *Langmuir* 8:283
25. De Battisti A, Lodi G, Cappadonia M, Battaglin G, Kötz R (1989) *J Electrochem Soc* 136:2596
26. Kameyama K, Tsukada K, Yahikozawa K, Takasu Y (1993) *J Electrochem Soc* 140:966
27. Kameyama K, Tsukada K, Yahikozawa K, Takasu Y (1994) *J Electrochem Soc* 141:643
28. Faita G, Fiori G (1972) *J Appl Electrochem* 2:31
29. Kötz R, Stucki S (1985) *J Electrochem Soc* 132:103
30. Kötz R, Stucki S (1986) *Electrochim Acta* 31:1311
31. Gorodetskii VV, Neburchilov VA, Pecherskii MM (1994) *Russ J Electrochem* 30:916
32. Kameyama K, Shohji S, Onoue S, Nishimura K, Yahikozawa K, Takasu Y (1993) *J Electrochem Soc* 140:1034
33. Takasu Y, Onoue S, Kameyama K, Murakami Y, Yahikozawa K (1994) *Electrochim Acta* 39:1993
34. Murakami Y, Miwa K, Ueno M, Ito M, Yahikozawa K, Takasu Y (1994) *J Electrochem Soc* 141:L118
35. Huang YS, Park HL, Pollak FH (1983) *Mater Res Bull* 17:1305
36. Trasatti S (1984) *Electrochim Acta* 29:1503
37. Cominellis Ch, Vercesi GP (1991) *J Appl Electrochem* 21:335
38. Vercesi GP, Salamin JY, Cominellis Ch (1999) *Electrochim Acta* 36:451
39. Mousty C, Fóti G, Cominellis Ch, Reid V (1991) *Electrochim Acta* 45:991
40. Fierro S, Nagel T, Baltruschat H, Cominellis Ch (2007) *Electrochim Commun* 9:1969
41. Ouattara L, Fierro S, Frey O, Koudelka M, Cominellis Ch (2009) *J Appl Electrochem* 39:1361